Available online at www.sciencedirect.com
ScienceDirect
Polymer 49 (2008) 588–598
polymer
www.elsevier.com/locate/polymer

Structural and thermal stabilization of isotactic polypropylene/organo-montmorillonite/poly(ethylene-*co*-octene) nanocomposites by an elastomer component

Tongchen Sun [a,b], Xia Dong [a,*], Kai Du [a,b], Ke Wang [c], Qiang Fu [c], Charles C. Han [a,*]

[a] *Beijing National Laboratory for Molecular Sciences, Joint Laboratory of Polymer Science and Materials, State Key Laboratory of Polymer Physics and Chemistry, Institute of Chemistry, CAS, Beijing 100080, China*
[b] *Graduate School of the Chinese Academy of Sciences, Beijing 100080, China*
[c] *Department of Polymer Science and Materials, Sichuan University, State Key Laboratory of Polymer Materials Engineering, Chengdu 610065, China*

Received 16 August 2007; received in revised form 13 November 2007; accepted 18 November 2007
Available online 21 November 2007

Abstract

Rheological and thermal properties of isotactic polypropylene (iPP)/organo-montmorillonite (OMMT)/poly(ethylene-*co*-octene) (PEOc) ternary nanocomposites and iPP/OMMT binary nanocomposites were studied by X-ray diffraction (XRD), rheometry, thermogravimetric analysis (TGA) and scanning electron microscopy (SEM) in this paper. The clay layers were mainly intercalated and partially exfoliated and well dispersed in these nanocomposites with the help of maleic anhydride modified polypropylene (PP*g*MA). Clay layers were mainly localized close to/inside the PEOc-rich phase from the direct observation of morphological study. A compact and stable network structure was formed in ternary composites when clay content was 2 phr (parts per hundred parts of iPP/PP*g*MA) or higher, which resulted in the lower stress relaxation rate and a pseudo-solid like behavior in low frequency region. Compared with iPP/OMMT composites, iPP/OMMT/PEOc composites had a much stronger ability to resist thermal decomposition. In another word, combining with the filler network, PEOc greatly improved the structural and thermal stabilities of iPP/OMMT nanocomposites.

Keywords: iPP/OMMT/PEOc ternary composites; Physical structural stability; Thermal stability

1. Introduction

In recent years, polymer-layered silicate nanocomposites (PLSNs) have drawn a lot of attention because of their academic and industrial importance [1–4]. Up to now, many kinds of matrix polymers of PLSN systems have been studied, such as nylon [5–8], polypropylene [9–11], polyethylene [12], polystyrene [13], poly(ethylene oxide) [14–16] and polystyrene/polyisoprene block copolymer [17] clay nanocomposites. Among these the polypropylene/clay nanocomposites are of special interest due to their outstanding industrial importance. Polypropylene with improved properties, such as enhanced mechanical strength, high thermal stability, low gas permeability, increased electric conductivity, can fulfill extensive industrial needs as automotive, barrier and packaging materials.

Therefore great attentions had been paid to the polypropylene/organoclay nanocomposites in the past decade. The nanocomposites were mainly prepared by two methods: in situ polymerization and melt blending. Kawasumi et al. [2] were the first to prepare polypropylene/clay nanocomposites by direct melt compounding of PP with inorganic montmorillonite (MMT) in the presence of maleic anhydride (MA) modified polypropylene oligomer as a compatibilizer. In this case clay layers were well dispersed in the base resin, which could help to improve the properties of the

* Corresponding authors. Tel.: +86 10 82618089; fax: +86 10 62521519.
E-mail addresses: xiadong@iccas.ac.cn (X. Dong), c.c.han@iccas.ac.cn (C.C. Han).

0032-3861/$ - see front matter © 2007 Elsevier Ltd. All rights reserved.
doi:10.1016/j.polymer.2007.11.033

nanocomposites. Since then melt blending became the dominating method to develop the polypropylene nanocomposites industrially. After that, researchers paid more attention to the dispersion of clay layers and morphology of the materials in order to understand the mechanism of the polymer–clay layers' interaction and also the connections between the macroscopic properties and the microscopic structures. Several techniques were often used to obtain the microscale information and interacting mechanism, such as X-ray diffraction, differential scanning calorimetry (DSC), transmission electron microscopy (TEM) and rheometry [10,18–23]. Particularly, a lot of information could be obtained from the rheological measurements to assess the state of clay layers' dispersion in the bulk state as well as in suspensions, since rheological results were very sensitive to the structure, particle size, shape, and surface characteristics of the dispersed phase. Krishnamoorti and Giannelis [24] and Ren et al. [17] intensively examined the melt rheology of PLSNs, and found a pseudo-solid like behavior in dynamic linear viscoelastic response of those composites. According to their investigation, a three-dimensional filler network structure was formed from the randomly oriented clay layers as the clay content reached a certain value in the nanocomposites. The clay layers were incapable of free rotation due to physical jamming and connecting with the nanoscale dispersed fillers [25]. Solomon et al. [26] and Gu et al. [27] also found the similar behavior in terminal region, and the power law exponents ($G' \propto \omega^2$ and $G'' \propto \omega$) were decreased gradually with the increase of clay content.

It was reported that the addition of organoclay greatly improved the mechanical and thermal properties of polypropylene [2,19,21,22]. However, further investigations showed that an obvious disadvantage of PP and PP/clay nanocomposites existed. This major deficiency was a low impact resistance, particularly at low temperatures, which was caused by its relatively high glass transition temperature (T_g). In order to overcome this problem, the addition of an elastomer was an appropriate way for toughening the PP/organoclay composites. There were many studies in the last 10 years about this toughening method [12,29,30]. Many elastomers had been used: ethylene–propylene–diene monomer (EPDM) was the most traditional selection but recently PEOc became the new choice. The ternary nanocomposites comprising iPP, organoclay and elastomer were usually examined from the aspect of mechanical measurements [28–30]. The toughness effect of elastomer was confirmed by the results from Lim et al. [31] and Ma et al. [32]. However, little information about the microscale or mesoscale structures was available in previous studies. Since microscale structure was a dominant factor determining the macroscale properties, we wanted to know the answers to the following questions: how were such three components interacting with each other? What were the structure and the morphology of the ternary nanocomposites? And how were they related to the properties?

In this study, we focused our attention mainly on the interacting mechanism of these three components and the improved properties of the iPP/OMMT/PEOc ternary nanocomposites. Rheology was the main technique we used to decipher these questions. In rheological measurements we compared the results of iPP/OMMT composites with those of iPP/OMMT/PEOc composites and obtained some conclusions about the effect of elastomer, organoclay and temperature. Then thermal measurements provided us with some complementary data. Finally, with the combination of XRD and SEM results, the dispersion and distribution of clay layers were examined and the interacting mechanism of these three components could be deduced.

2. Experimental

2.1. Materials

A commercially available isotactic polypropylene (trade marked as T30s, Yan Shan Petroleum China) with $M_w = 4.0 \times 10^5$ g/mol, polydispersity index (PDI) = 4.7, and density of 0.91 g/cm^3 was used as one component of the matrices. Maleic anhydride modified polypropylene with $M_w = 2.1 \times 10^5$ g/mol, PDI = 3.2 and the content of MA 0.9 wt% was used as the compatibilizer, which was purchased from Chen Guang Co. (Sichuan, China). Sodium montmorillonite (MMT) with a cation exchange capacity of 68.8 mmol/100 g (Renshou, Sichuan, China) was organically modified through ion-exchange reaction with dioctadecyl dimethylammonium bromide. The individual MMT layer was several nanometers in thickness and 100 nm in diameter. An elastomer PEOc with $M_w = 1.4 \times 10^5$ g/mol, PDI = 2.2 was used as the other component of the matrices, which was purchased from Dupont Dow Elastomer with the trade mark as Engage 8150. All chemical reagents used in the experiments were of analytical grade.

2.2. Preparation of the composites

Firstly a batch of pellets with the composition of iPP/PP*g*MA/OMMT (90/10/5 by weight) and another batch of pellets with the composition of iPP/PP*g*MA (90/10 by weight) were melt-blended in a TSSJ-2S co-rotating twin-screw extruder. The temperatures of the extruder were maintained at 170 °C, 190 °C, 200 °C and 195 °C from hopper to die, and the screw speed was 110 r/min. Then a series of iPP/PP*g*MA/OMMT (90/10/*x* by weight, $x = 0$, 0.5, 1, 2, 3, 4, 5) nanocomposites were obtained through adding iPP/PP*g*MA to dilute the as-prepared composites with 5 phr OMMT. And another series of iPP/PP*g*MA/OMMT/PEOc (90/10/*x*/*y* by weight, $x = 0$, 0.5, 1, 2, 3, 4, 5; $y = 0$, 5, 15, 25) composites were prepared through adding iPP/PP*g*MA and PEOc to the as-prepared composites with 5 phr OMMT. These two kinds of pellets with different compositions were dissolved in xylene (composites/xylene = 1 g:20 mL) at around 130 °C and then precipitated in cool methanol. After the precipitation the composites were dried in the vacuum oven at 45 °C. Then the prepared samples were marked as PPCN*x* for iPP/PP*g*MA/OMMT and PPCN*x*OE15 for iPP/PP*g*MA/OMMT/PEOc nanocomposites.

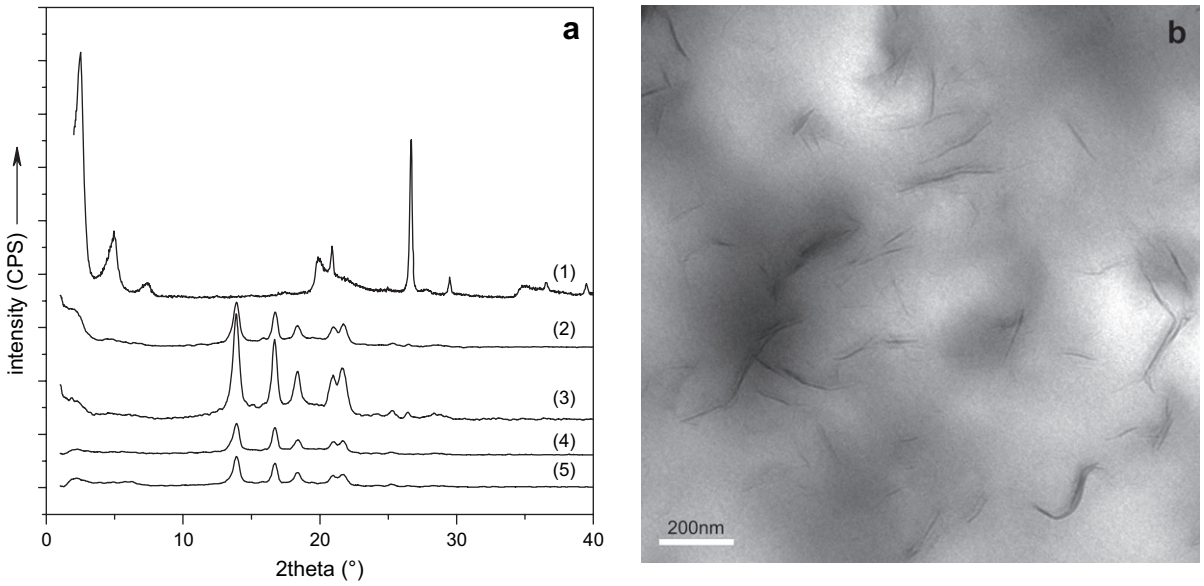

Fig. 1. (a) XRD patterns of (1) OMMT, (2) PPCN5OE15, (3) PPCN5, (4) PPCN2OE15 and (5) PPCN2; and (b) TEM image of PPCN5.

2.3. Measurements and characterization

2.3.1. X-ray diffraction

XRD experiments were carried out with a Rigaku (Japan) D/max 2400 diffractometer. The X-ray beam was derived from nickel-filtered Cu Kα ($\lambda = 0.154$ nm) radiation in a sealed tube operated at 40 kV and 200 mA. The test samples were prepared by compression molding and the experiments were performed in the angle range 1°–40°, at a scanning rate of 6°/min and a scanning step of 0.02°. These experiments were conducted to determine the dispersion of clay layers in the iPP or iPP/PEOc matrices and the crystallization of iPP in the nanocomposites.

2.3.2. Transmission electron microscopy

The samples for TEM analysis were prepared by ultra cryomicrotomy at −60 °C with a thickness of 100 nm using a Leica EM UC6 ultramicrotome. The microscopic study was conducted with a JEOL (JEM-2200FS) transmission electron microscope, operating at an accelerating voltage of 200 kV.

2.3.3. Rheological measurement

All rheological experiments were conducted with an Advanced Rheometric Expansion System (ARES, Rheometric Scientific, NJ) which was a strain-controlled rheometer with a parallel-plate fixture (25 mm diameter). Disk samples were prepared by compression molding with the thickness of 1.2 mm and diameter of 25 mm. The gap between two parallel plates was maintained at 0.9 mm for all rheological measurements. Dynamic strain sweep experiments were carried out at 220 °C and 100 rad/s to distinguish the linear viscoelastic behavior region from the nonlinear viscoelastic behavior region, and dynamic frequency sweep experiments were followed. Storage modulus and loss modulus (G' and G'') as a function of angular frequency (ω) (ranging from 0.01 rad/s to 100 rad/s) at 180–220 °C in linear viscoelastic region were measured. Stress relaxation experiments were also carried out with step strain of 200% at 190 °C. All the measurements were carried out under a nitrogen atmosphere to avoid oxidative degradation of the specimens.

2.3.4. Differential scanning calorimetry

A Perkin–Elmer DSC-7 was used to determine the influence of OMMT and PEOc on the crystallization and melting behaviors of the samples. The test samples (about 4 mg) were first heated from 50 °C to 200 °C at a heating rate of 10 °C/min and then held at 200 °C for 5 min to eliminate the thermal and mechanical history. Then the cooling process was studied from 200 °C to 50 °C at a cooling rate of 10 °C/min to investigate the crystallization behavior. Then the samples were held at 50 °C for 5 min and then heated to 200 °C again at a heating rate of 10 °C/min to study the melting behavior. All the measurements were conducted under a nitrogen cover with a flow rate of 20 mL/min.

2.3.5. Thermogravimetric analysis

A Perkin–Elmer thermal gravimetric analyzer (TGA-7) was used to investigate the effect of clay layers and PEOc on the high temperature decomposition of these composites. Samples (about 4 mg) were heated under a nitrogen atmosphere with a flow rate of 20 mL/min from 30 °C to 650 °C at a heating rate of 20 °C/min.

Table 1
Interlayer spacings of hybrid materials derived from XRD

Sample	The layer spacing (nm)	Sample	The layer spacing (nm)
PPCN5	4.7	PPCN5OE15	4.9
PPCN2	4.2	PPCN2OE15	4.2
OMMT	3.5	–	–

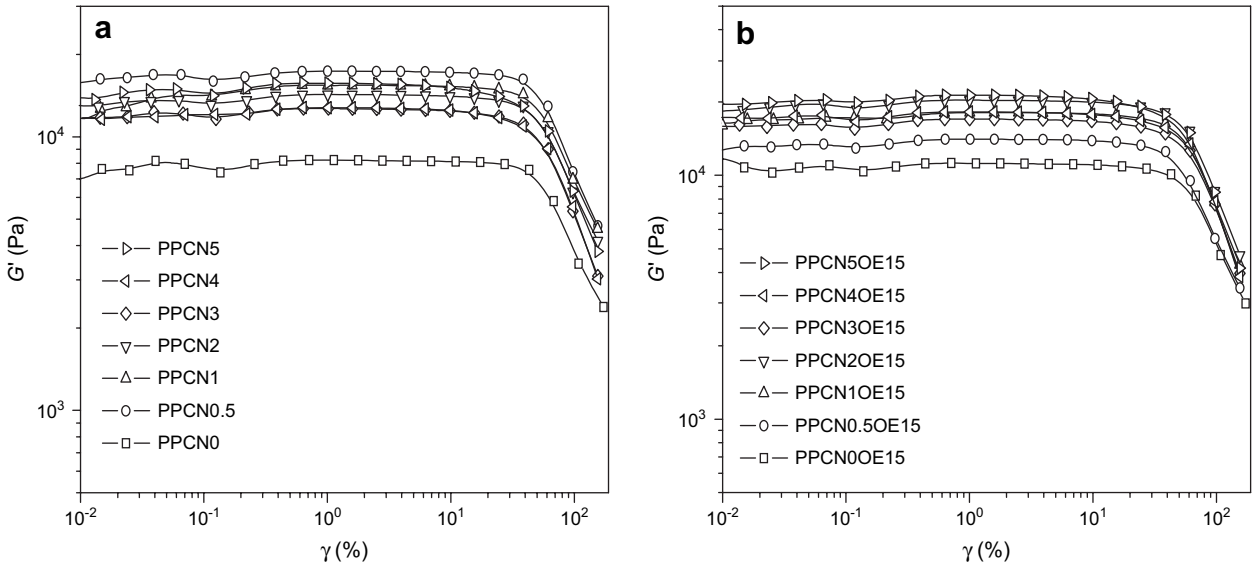

Fig. 2. Dynamic strain sweep spectra of (a) PPCN*x* and (b) PPCN*x*OE15 nanocomposites at $\omega = 100$ rad/s and $T = 220$ °C.

2.3.6. Scanning electron microscopy

Some selected samples were cryogenically fractured in liquid nitrogen and then etched in xylene at ambient temperature for 24 h. Then the fractured surfaces of samples were coated with platinum prior to examination by a scanning electron microscope. A JEOL (JSM 6700F) scanning electron microscope was used with an operating voltage of 5 kV for this study.

3. Results and discussion

3.1. The dispersion of clay layers in the nanocomposites

The X-ray diffraction patterns of OMMT, PPCN2, PPCN2OE15, PPCN5 and PPCN5OE15 nanocomposites are shown in Fig. 1(a). The largest average interlayer distance of neat OMMT was about 3.5 nm and there still existed a large amount of OMMT with small interlayer distance, which was deduced from the minimum diffraction angle of OMMT curve. The interlayer distances of the other four nanocomposites are listed in Table 1. There were no big differences among the interlayer distances of these four nanocomposites, which indicated that the existence of PEOc in PPCN*x*OE15 nanocomposites had almost no effect on clay gallery in the polymer matrices. But the interlayer distances of these four samples were all larger than that of the primary OMMT. This meant that after the blending process polymer chains including iPP and PEOc did intercalate into the organoclay layers and increased the gallery distance. The conclusion could be explained by the following arguments. In small angle region of

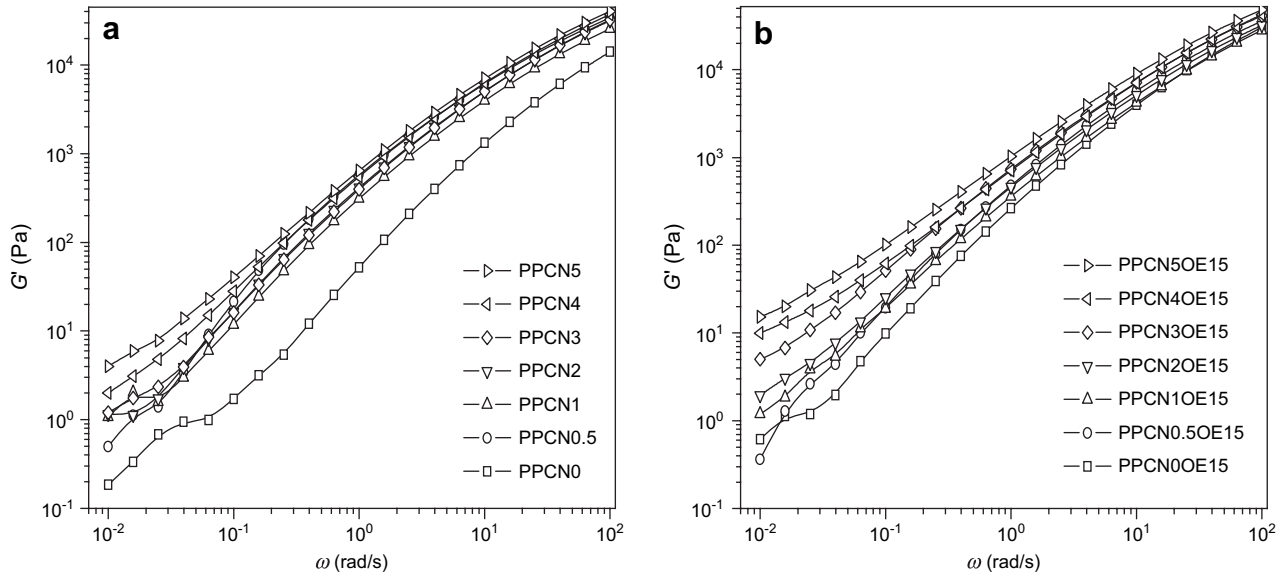

Fig. 3. Storage modulus as a function of frequency for (a) PPCN*x* and (b) PPCN*x*OE15 nanocomposites at 190 °C.

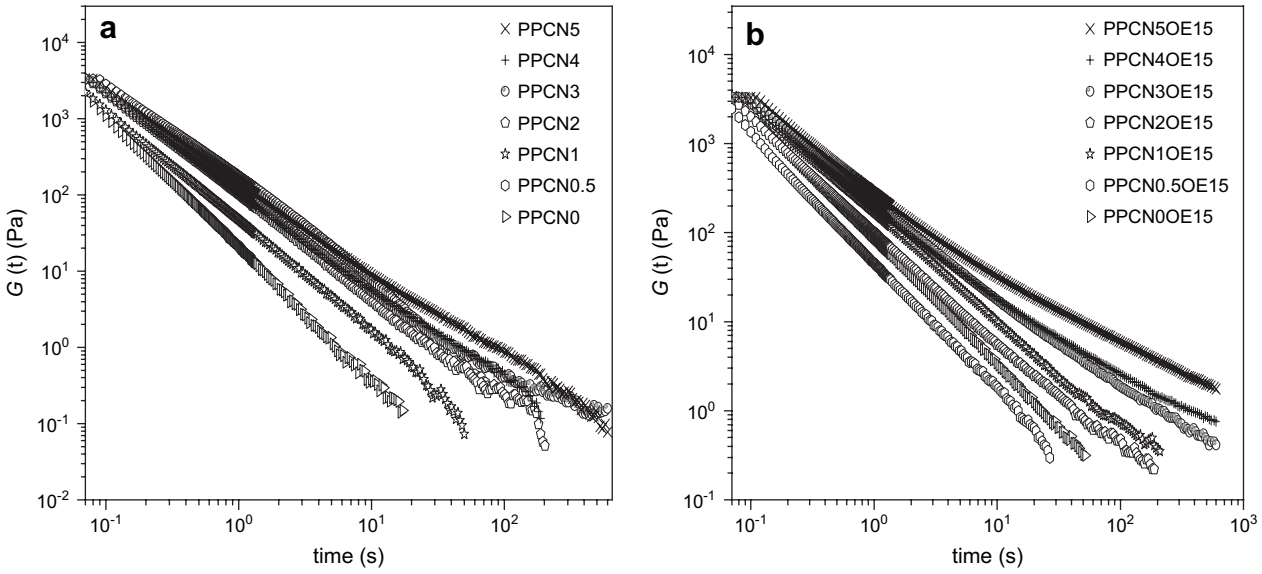

Fig. 4. Stress relaxation spectra of (a) PPCN*x* and (b) PPCN*x*OE15 nanocomposites with 200% step strain at 190 °C.

the X-ray diffraction patterns there were significant differences between the curve of OMMT and those of other four nanocomposites. Not only the position and shape of these diffraction peaks were shifting and broadening but also the intensities were greatly reduced, which indicated that the state of organoclay in the nanocomposites was dramatically different from that of neat organoclay. TEM image of PPCN5 in Fig. 1(b) showed that organoclay layers were intercalated and even partially exfoliated by polymer chains.

Meanwhile, in 10°–25° region, the peak position and shape of these four curves of nanocomposites were almost the same, which indicated that there were no big differences in crystal form of polypropylene. So the addition of PEOc had no big effect on the crystallization behavior of polypropylene.

In a word, after the blending process, organoclay layers were intercalated and even partially exfoliated and well dispersed in the polymer matrices with the help of PP*g*MA. However, PEOc did not affect the intercalation and the exfoliation of the PPCN*x* nanocomposites beyond what had already happened during the clay dispersion and crystallization of iPP in the PPCN*x*.

3.2. Rheological behaviors of the nanocomposites

Rheological measurements were very sensitive to the shape, size and dispersion of fillers in the nanocomposites, so an oscillatory shear measurement was used to characterize the dynamic rheological properties of PPCN*x* binary and PPCN*x*OE*y* ternary nanocomposites. First, the dynamic strain sweep measurements were conducted for all samples in order to choose an appropriate strain for the investigation of the linear viscoelastic behaviors of these nanocomposites. Fig. 2 shows the strain dependence of storage modulus (G') of all these samples at 220 °C with a frequency of 100 rad/s. G' started to drop drastically when strain exceeded 30%, which indicated that the structure of the material was destroyed. Therefore a strain of 5% which was well within this 30% limit was chosen as the appropriate strain to investigate the linear viscoelastic behaviors of these nanocomposites.

3.2.1. Rheological behaviors and structural stability

Fig. 3 shows the results of dynamic frequency sweep measurements of PPCN*x* and PPCN*x*OE15 nanocomposites at 190 °C. Storage modulus of polypropylene was generally increased with the addition of organoclay as shown in Fig. 3(a). In low frequency region a more obvious increase of G' was observed with the increase of clay concentration. The slope of G' vs. ω curve in terminal region became smaller with the increase of clay concentration when it was more than 2 phr. The system exhibited a pseudo-solid like behavior in low frequency region when organoclay content was 2 phr or higher, which could be explained by the three-dimensional filler network theory proposed by Krishnamoorti and Silva. When clay content reached a certain value in the nanocomposites, the clay layers were incapable of free rotation due to physical jamming and connecting with each other and so the structure was formed from the random oriented clay layers [25]. This three-dimensional filler network structure played a significant role in many properties of PPCN*x* nanocomposites.

Fig. 3(b) shows storage modulus of PPCN*x*OE15 nanocomposites as a function of frequency. After PEOc was added, the change of slope of G' vs. ω curve in low frequency region was more obvious, which indicated that PEOc played an additional role in the rheological properties of PPCN*x*OE15 nanocomposites. Probably PEOc interacted with the three-dimensional filler network, which helped to influence the low frequency behaviors of PPCN*x*OE15 greatly.

Fig. 4 shows the stress relaxation spectra of these samples which were conducted with step strain of 200% at 190 °C. Stress relaxation time was increased with the increase of organoclay content in Fig. 4(a). When clay content was 2 phr

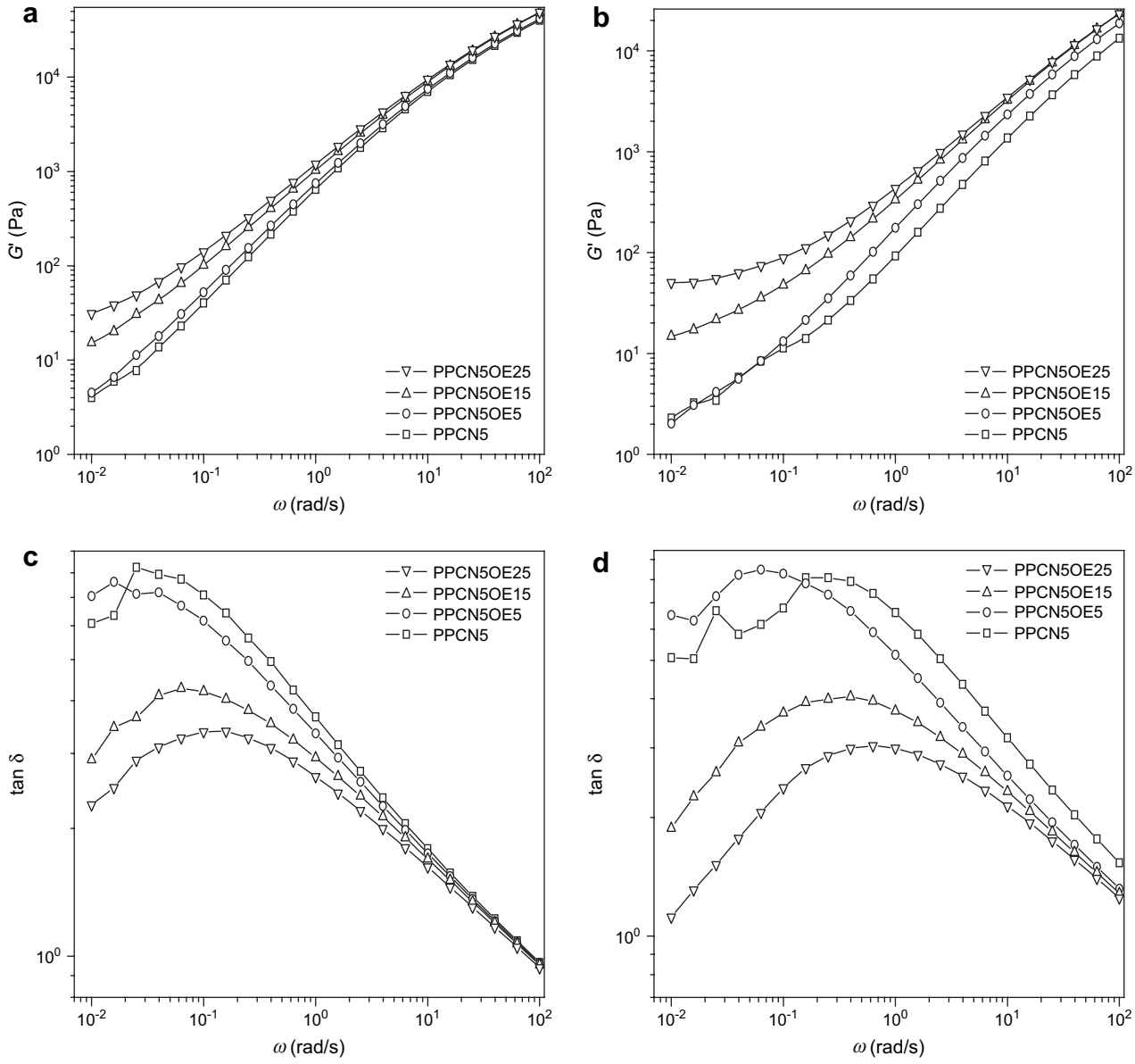

Fig. 5. Storage modulus and loss tangent as a function of frequency for PPCN5OE*y* at 190 °C (a and c) and 220 °C (b and d).

or higher, the stress relaxation time of these binary nanocomposites was significantly higher than those at lower clay concentrations, but insignificantly different among themselves, which indicated that the relaxation modes of the high clay concentration samples were similar and the three-dimensional filler network dominated the relaxation process. The stress relaxation spectra of PPCN*x*OE15 nanocomposites are shown in Fig. 4(b). PEOc component greatly influenced the stress relaxation rates especially when clay content was above 2 phr. For these samples the stress relaxation time was much longer (more than two orders of magnitudes longer), which implied that PEOc was participating in the formation of the network structure and influenced the stress relaxation modes and resulted in a better structural stability under external stress.

Both PPCN*x* and PPCN*x*OE15 nanocomposites are investigated in Figs. 3 and 4, and the factors that greatly influenced the rheological properties of these two kinds of nanocomposites could be obtained as follows:

(1) the effect of organoclay;
(2) the synergetic effect of organoclay and PEOc;
(3) the additional effect of PEOc.

These three main factors could significantly affect rheological behaviors and also some other properties of these nanocomposites. Temperature was another important factor and its effect on the structural stability of these nanocomposites was to be discussed later.

3.2.2. Elastomer content dependence

Fig. 5 shows the storage modulus and loss tangent of PPCN5OE*y* as a function of frequency at 190 °C and 220 °C. With the increase of PEOc content, the increase of

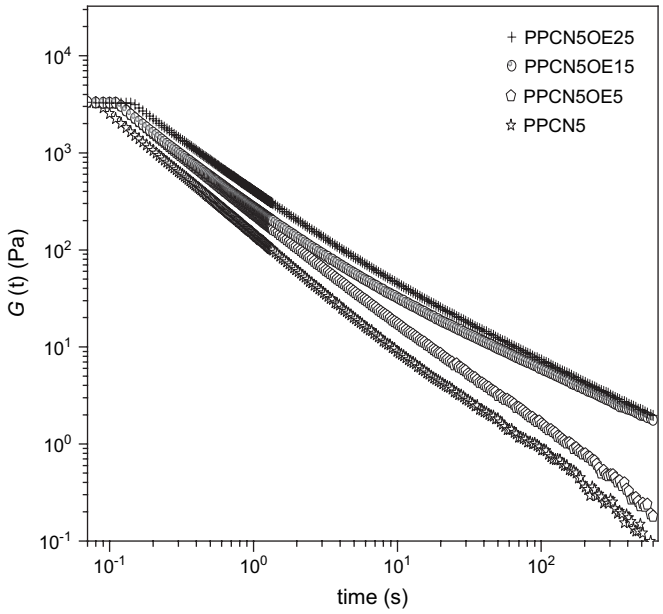

Fig. 6. Stress relaxation spectra of PPCN5OE*y* with 200% step strain at 190 °C.

G' (Fig. 5(a) and (b)) in terminal region was more obvious, and the slope of log G' vs. log ω curve changed to become smaller. In Fig. 5(c) and (d), the peak position of loss tangent, which was corresponding to the turning point of storage modulus, was shifted to higher frequency with the increase of PEOc content. These indicated that the addition of PEOc changed the low frequency storage modulus and slowed down the stress relaxation. It was speculated that the mechanism must have involved the interaction of clay layers together with the PP*g*MA and some iPP chains with the elastomeric PEOc chains and preferentially interacted with the PEOc-rich domains. This might be caused by some preferred interaction with the side group of the octene or due to the elastomeric nature of the PEOc. With the increase of PEOc content, the phase-separated PEOc-rich domains which might be either wrapping around the OMMT/PP*g*MA structures or absorbing these structures on the domain surfaces could easily promote the formation of a percolated structure with the continuous OMMT/PP*g*MA as the stress carrying part of the network.

Fig. 6 shows the stress relaxation spectra of PPCN5OE*y* which were conducted with 200% step strain at 190 °C. The stress relaxation rate became slower with the increase of PEOc content, which indicated that PEOc indeed participated in the formation of structure directly. PPCN5OE25 had similar stress relaxation rate as PPCN5OE15, which indicated that in these two nanocomposites the strength of network comprising clay layers and different amount of PEOc was essentially the same. This meant that a compact network might have been formed when PEOc content was about 15 phr in which the low frequency stress (or long relaxation mode) was carried by the OMMT/PP*g*MA network although it might be formed with the help of the phase-separated PEOc-rich domains.

3.2.3. Temperature dependence of the structural stability

Compared with that in Fig. 5(c), the peak position of loss tangent of the same sample in Fig. 5(d) shifted to higher frequency. This was caused by the temperature. Fig. 7 shows log G' vs. log ω curves for PPCN5 and PPCN5OE15 nanocomposites at different temperatures. The turning point of storage modulus of PPCN5 in Fig. 7(a) shifted to higher frequency with the increase of temperature, the same thing happened to G' of PPCN5OE15 in Fig. 7(b). This could be explained by the time–temperature superposition (TTS) principle. It was well known that time–temperature superposition was usually applied to homogeneous materials but not for multi-phase nanocomposite systems. log G' vs. log G'' curves

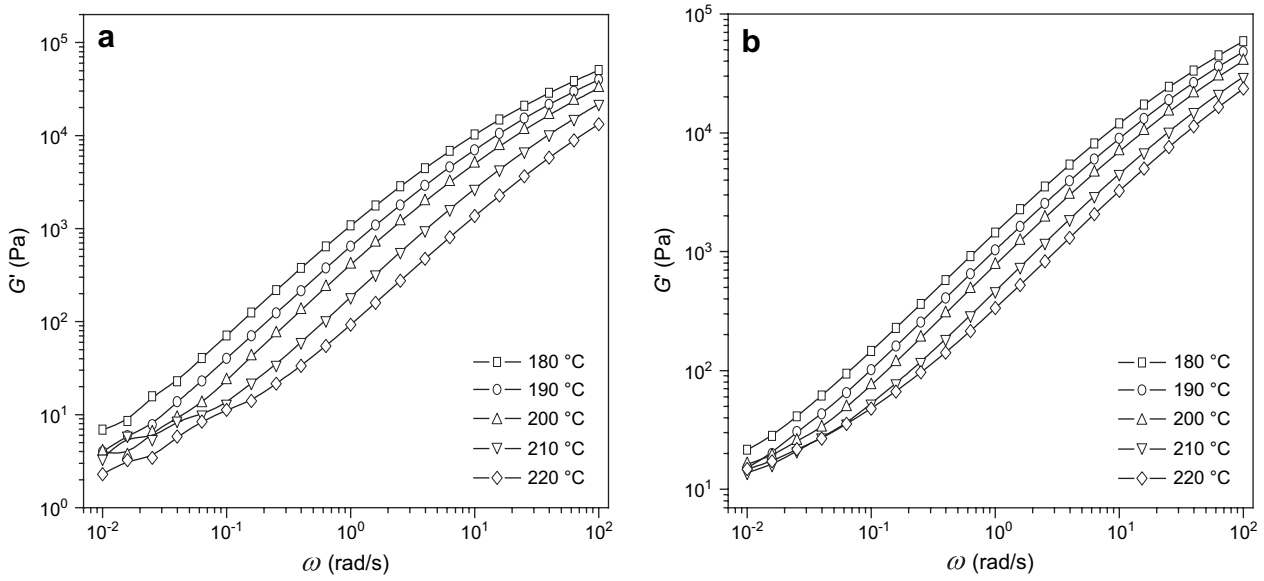

Fig. 7. Plots of log G' vs. log ω for (a) PPCN5 and (b) PPCN5OE15 at different temperatures.

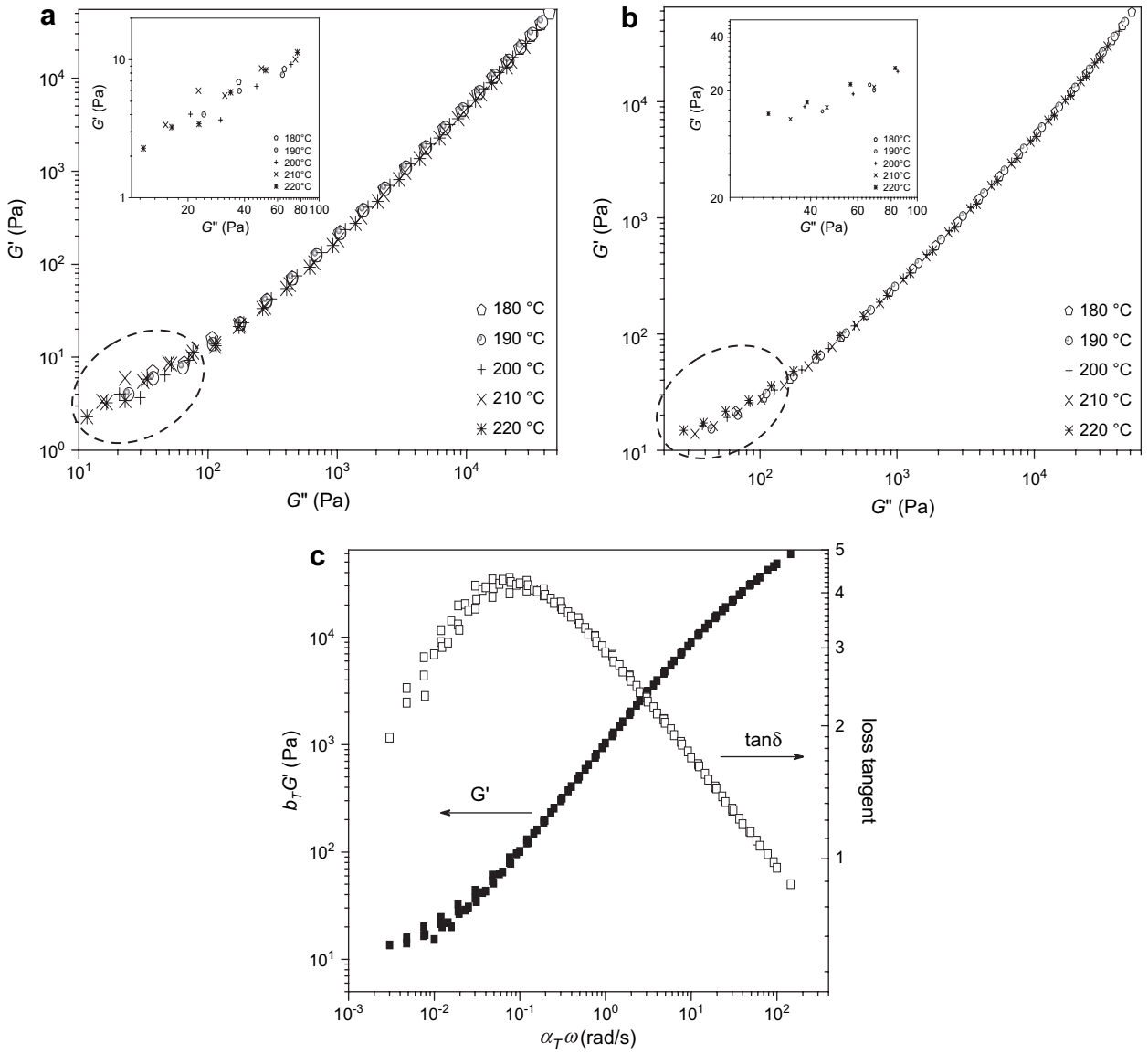

Fig. 8. Plots of log G' vs. log G'' for (a) PPCN5 and (b) PPCN5OE15, insets correspond to the marked curves by circles, and (c) time–temperature superposition master curves of PPCN5OE15.

(Han plot) of these two composites are shown in Fig. 8(a) and (b). Curves in the marked region were magnified and shown as insets in Fig. 8(a) and (b), respectively. It was noticeable that there was deviation in terminal region for PPCN5 while Han plot of PPCN5OE15 had no temperature dependence. So TTS was not applicable for PPCN5 nanocomposites, but it worked reasonably well for PPCN5OE15 nanocomposites. This implied that rheologically PPCN5OE15 behaved like a homogeneous material, and the TTS master curves are shown in Fig. 8(c).

3.3. Thermal stability

After mixing with organoclay and PEOc, the crystallization behavior and melting behavior of polypropylene were examined by DSC measurements. There was no significant change in the crystallization and melting behaviors of polypropylene in PPCN*x* nanocomposites or in PPCN*x*OE*y* nanocomposites. This meant that the addition of organoclay and PEOc did not change the crystallization and melting mechanism of the polypropylene.

Fig. 9(a) shows the TGA traces of PPCN*x* binary nanocomposites. With the increase of OMMT content the degradation temperatures of these samples increased. The ability of heat resistance of polypropylene was greatly enhanced by the addition of organoclay. In Fig. 9(b) we took two kinds of ternary nanocomposites as examples: PPCN0OE15 and PPCN4OE15. It was found that these two ternary nanocomposites had higher degradation temperature than the binary nanocomposites with the same clay content. The degradation temperature difference between PPCN0 and PPCN0OE15 was much bigger than that between PPCN4 and PPCN4OE15. The other ternary nanocomposites we investigated also showed improved heat resistance ability.

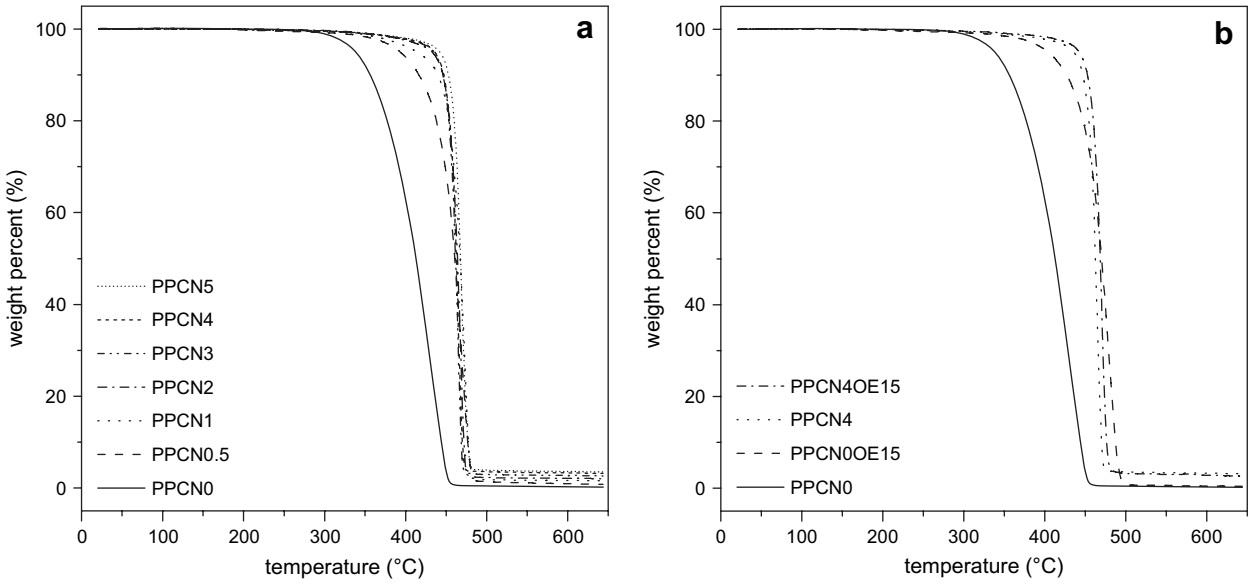

Fig. 9. TGA traces of (a) PPCN*x* binary nanocomposites and (b) PPCN0, PPCN0OE15, PPCN4 and PPCN4OE15.

In order to more clearly explain the thermal stability of these samples, the other two important parameters "5% weight loss temperature" and "onset temperature" were introduced. The onset temperature was defined as the temperature corresponding to the crossover of the tangent to the starting point and that to the inflection point of TGA curve. In Fig. 10(a), the temperature of 5% weight loss of PPCN*x* nanocomposites was increasing with the increase of organoclay concentration and reached to a plateau when the organoclay concentration was 2 phr or higher. The "5% weight loss temperature" of ternary nanocomposites was higher than that of binary nanocomposites with the same OMMT content. The changing trends of "5% weight loss temperature" of these two kinds of nanocomposites were similar. So were those of "onset temperature". This indicated that the basic stabilization effect was caused by the addition of organoclay and was similar for both binary and ternary nanocomposites. In Fig. 10 both the "5% weight loss temperature" and "onset temperature" were increasing with the increase of organoclay concentration, which had been explained by Zanetti et al. [33]. They thought that in the clay-filled nanocomposites there should be a barrier labyrinth effect to diffusion of degradation products from the bulk to the gas phase. Due to the physical barrier effect, the thermal stability was strongly enhanced by adding fillers to the polymer matrices.

In Fig. 10, the "5% weight loss temperature" and "onset temperature" of the ternary nanocomposites were both higher than those of the binary nanocomposites, which was caused by

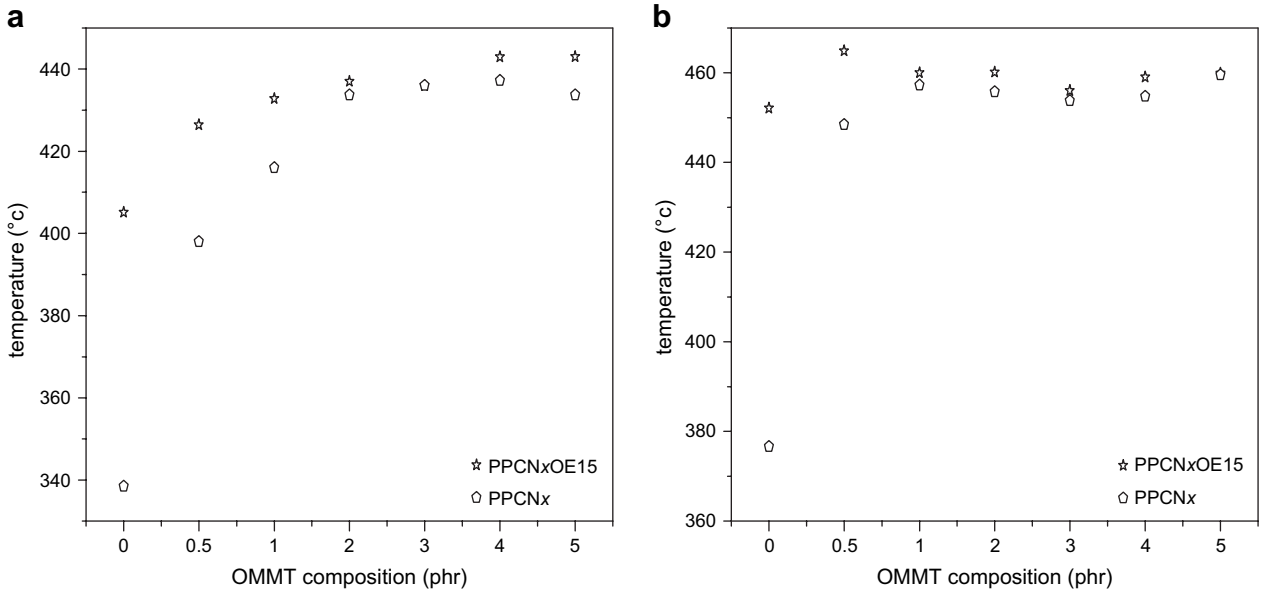

Fig. 10. (a) The temperature of 5% weight loss and (b) onset temperature of PPCN*x* and PPCN*x*OE15 nanocomposites.

Table 2
The degradation temperatures of PPCN0 and neat PEOc derived from TGA

Sample	The 5% weight loss temperature (°C)	The onset temperature (°C)	The residue percent (%)
PPCN0 (iPP/PP*g*MA)	338.5	376.6	0.26
PEOc	382.3	448.0	0.45

the addition of PEOc. It was conjectured that a more compact network comprising clay layers and PEOc chains was formed in PPCN*x*OE15 ternary nanocomposites, hence the network structure was playing a positive role in the formation of a more stable and stronger physical barrier. Furthermore, neat PEOc had a higher degradation temperature than PPCN0 (iPP/PP*g*MA), which is shown in Table 2. This natural property also helped to improve the thermal stability and heat resistance of PPCN*x*OE15 ternary nanocomposites. This point could be affirmed by the bigger degradation temperature difference between PPCN0 and PPCN0OE15 than that between PPCN4 and PPCN4OE15 in Fig. 9(b).

3.4. Clay layer distribution and morphology of these nanocomposites

SEM examination was conducted on the cross-section of samples to further investigate the distribution of clay layers in the nanocomposites. Fig. 11 shows the SEM images of PPCN5OE*y* nanocomposite samples which were etched with xylene to remove the PEOc-rich phase. With the increase of PEOc content not only the number of holes where PEOc-rich phase was removed but also the size of the holes increased. Meanwhile, the number of clay layers which still existed on the fractured and etched surfaces was decreased. These existing organoclay layers were distributed close to the PEOc-rich phase of PPCN5OE*y* nanocomposites, as shown in Fig. 11(b)–(d). It indicated that in the ternary nanocomposites the organoclay layers were mainly localized close to/inside the PEOc-rich phase. Similar observations had been reported in nylon-66/organoclay/SEBS-*g*-MA system by Dasari et al. [7,8]. In their case, the distribution of organoclay was caused mainly by the blending procedure, but in our case it was probably caused by the interaction between the organoclay and the PEOc elastomer. This was in accord with the speculated mechanism drawn from rheological and TGA measurements: a percolated network structure was formed, which comprised clay layers and PEOc domains in the PPCN*x*OE*y* ternary nanocomposites. This more compact network structure could help to improve many properties of polypropylene, such as structural stability and heat resistance.

4. Conclusion

Rheological and thermal properties of iPP/OMMT/PEOc ternary nanocomposites were investigated in this work. Through the co-precipitation process organoclay layers were well dispersed in the polymer matrices with the help of

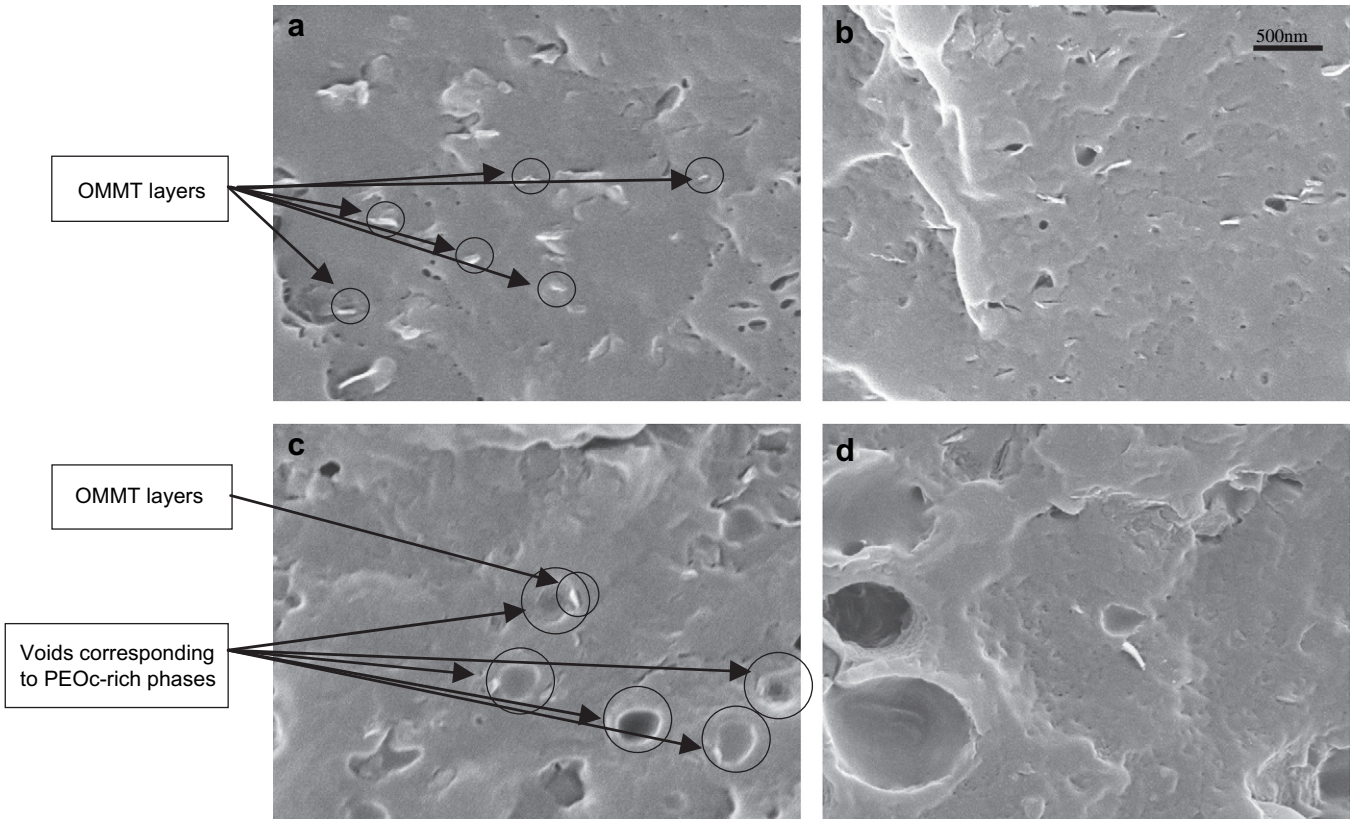

Fig. 11. SEM images of fractured and etched surfaces of (a) PPCN5, (b) PPCN5OE5, (c) PPCN5OE15 and (d) PPCN5OE25 nanocomposites.

PP*g*MA with or without the addition of PEOc. The addition of PEOc into iPP/OMMT helped to increase the storage modulus in general and influenced the low frequency storage modulus and stress relaxation rate, especially for sample PPCN5OE15. This was attributed to a compact and stable three-dimensional network structure consisting of organoclay layers and PEOc in iPP/OMMT/PEOc ternary composites, which helped to improve the rheological stability and also thermal stability of polypropylene.

Acknowledgements

The authors thank the generous financial support by following grants: National Natural Sciences Foundation of China, Grant Nos. 20490220 and 20574081 and the National Basic Research Program (973 program) No. 2003CB615600 of MOST.

References

[1] Ray SS, Okamoto M. Prog Polym Sci 2003;28:1539.
[2] Kawasumi M, Hasegawa N, Kato M, Usuki A, Okada A. Macromolecules 1997;30:6333.
[3] Krishnamoorti R, Yurekli K. Curr Opin Colloid Interface Sci 2001;6:464.
[4] Giannelis EP. Adv Mater 1996;8:29.
[5] Tung J, Gupta RK, Simon GP, Edward GH, Bhattacharya SN. Polymer 2005;46:10405.
[6] Chiu FC, Lai SM, Chen YL, Lee TH. Polymer 2005;46:11600.
[7] Dasari A, Yu ZZ, Mai Y-W. Polymer 2005;46:5986.
[8] Dasari A, Yu ZZ, Yang MS, Zhang QX, Xie XL, Mai Y-W. Compos Sci Technol 2006;66:3097.
[9] Zhang Q, Wang Y, Fu Q. J Polym Sci Part B Polym Phys 2003;41:1.
[10] Koo CM, Kim SO, Chung IJ. Macromolecules 2003;36:2748.
[11] Vermogen A, Masenelli-Varlot K, Seguela R, Duchet-Rumeau J, Boucard S, Prele P. Macromolecules 2005;38:9661.
[12] Chow WS, Bakar AA, Mohd Ishak ZA, Karger-Kocsis J, Ishiaku US. Eur Polym J 2005;41:687.
[13] Zhong Y, Zhu ZY, Wang SQ. Polymer 2005;46:3006.
[14] Lin-Gibson S, Schmidt G, Kim H, Han CC, Hobbie EK. J Chem Phys 2003;119:8080.
[15] Lin-Gibson S, Kim H, Schmidt G, Han CC, Hobbie EK. J Colloid Interface Sci 2004;274:515.
[16] Dundigalla A, Lin-Gibson S, Ferreiro V, Malwitz MM, Schmidt G. Macromol Rapid Commun 2005;26:143.
[17] Ren JX, Silva AS, Krishnamoorti K. Macromolecules 2000;33:3739.
[18] Lee KM, Han CD. Macromolecules 2003;36:7165.
[19] Bartholmai M, Schartel B. Polym Adv Technol 2004;15:355.
[20] Morgan AB, Gilman JW. J Appl Polym Sci 2003;87:1329.
[21] Koo CM, Kim MJ, Choi MH, Kim SO, Chung IJ. J Appl Polym Sci 2003;88:1526.
[22] Marchant D, Jayaraman K. Ind Eng Chem Res 2002;41:6402.
[23] Galgali G, Ramesh C, Lele A. Macromolecules 2001;34:852.
[24] Krishnamoorti R, Giannelis EP. Macromolecules 1997;30:4097.
[25] Krishnamoorti R, Silva AS. In: Pinnavaia TJ, Brall GW, editors. Polymer–clay nanocomposites. New York: John Wiley & Sons; 2000. p. 315.
[26] Solomon MJ, Almusallam AS, Seefeldt KF, Somwangthanaroj A, Varadan P. Macromolecules 2001;34:1864.
[27] Gu SY, Ren J, Wang QF. J Appl Polym Sci 2004;91:2427.
[28] Maiti M, Bandyopadhyay A, Bhowmick AK. J Appl Polym Sci 2006;99:1645.
[29] Tjong SC, Bao SP, Liang GD. J Polym Sci Part B Polym Phys 2005;43:3112.
[30] Wang X, Pang SL, Yang JH, Yang F. Trans Nonferrous Met Soc China 2006;16:s524.
[31] Lim JW, Hassan A, Rahmat AR, Wahit MU. J Appl Polym Sci 2006;99:3441.
[32] Ma XY, Liang GZ, Lu HJ, Liu HL, Huang Y. J Appl Polym Sci 2005;97:1907.
[33] Zanetti M, Camino G, Reichert P, Mülhaupt R. Macromol Rapid Commun 2001;22:176.